PNAS RESEARCH ARTICLE | NEUROSCIENCE OPEN ACCESS

MicroRNA-335-5p suppresses voltage-gated sodium channel expression and may be a target for seizure control

Mona Heiland[a,b], Niamh M. C. Connolly[a,b], Omar Mamad[a,b], Ngoc T. Nguyen[a,b], Jaideep C. Kesavan[a,b], Elena Langa[a,b], Kevin Fanning[a,b], Albert Sanfeliu[a,b], Yan Yan[c,d,e], Junyi Su[c,d], Morten T. Venø[c,d,e], Lara S. Costard[f,g,h], Valentin Neubert[f], Tobias Engel[a,b], Thomas D. M. Hill[a,b], Thomas M. Freiman[g,i], Arun Mahesh[j], Vijay K. Tiwari[j,k,l,m], Felix Rosenow[f,g,h], Sebastian Bauer[f,g,h], Jørgen Kjems[c,d], Gareth Morris[a,b,n,1], and David C. Henshall[a,b,1,2]

Edited by Hee-Sup Shin, Institute for Basic Science, Daejeon, South Korea; received October 6, 2022; accepted May 17, 2023

There remains an urgent need for new therapies for treatment-resistant epilepsy. Sodium channel blockers are effective for seizure control in common forms of epilepsy, but loss of sodium channel function underlies some genetic forms of epilepsy. Approaches that provide bidirectional control of sodium channel expression are needed. MicroRNAs (miRNA) are small noncoding RNAs which negatively regulate gene expression. Here we show that genome-wide miRNA screening of hippocampal tissue from a rat epilepsy model, mice treated with the antiseizure medicine cannabidiol, and plasma from patients with treatment-resistant epilepsy, converge on a single target—miR-335-5p. Pathway analysis on predicted and validated miR-335-5p targets identified multiple voltage-gated sodium channels (VGSCs). Intracerebroventricular injection of antisense oligonucleotides against miR-335-5p resulted in upregulation of *Scn1a*, *Scn2a*, and *Scn3a* in the mouse brain and an increased action potential rising phase and greater excitability of hippocampal pyramidal neurons in brain slice recordings, consistent with VGSCs as functional targets of miR-335-5p. Blocking miR-335-5p also increased voltage-gated sodium currents and *SCN1A, SCN2A*, and *SCN3A* expression in human induced pluripotent stem cell-derived neurons. Inhibition of miR-335-5p increased susceptibility to tonic-clonic seizures in the pentylenetetrazol seizure model, whereas adeno-associated virus 9-mediated overexpression of miR-335-5p reduced seizure severity and improved survival. These studies suggest modulation of miR-335-5p may be a means to regulate VGSCs and affect neuronal excitability and seizures. Changes to miR-335-5p may reflect compensatory mechanisms to control excitability and could provide biomarker or therapeutic strategies for different types of treatment-resistant epilepsy.

epilepsy | noncoding RNA | antisense oligonucleotides | adeno-associated virus | drug resistance

Significance

Despite the clinical availability of over 30 antiseizure medications, around 30% of people with epilepsy do not achieve seizure freedom. MicroRNAs are small noncoding RNAs which negatively regulate protein levels by binding to target mRNAs. Here, we identified the brain-enriched miR-335-5p to be commonly altered in three heterogeneous microRNA profiling datasets. Bidirectional modulation of miR-335-5p identified a potential homeostatic role of miR-335-5p in neuronal excitability involving voltage-gated sodium channels. Electrophysiological and in vivo approaches revealed pro-epileptic effects of miR-335-5p inhibition, whereas overexpression of miR-335-5p resulted in antiepileptic activity. Overall, targeting miR-335-5p could provide an approach in the modulation of neuronal excitability, with possible therapeutic applications in treatment-resistant epilepsies and other neurological diseases.

Epilepsy is one of the most common neurological diseases, affecting ~65 million people worldwide, and is characterized by spontaneous recurrent seizures caused by excessive or hypersynchronous neuronal activity (1). Currently, over 30 antiseizure medications (ASMs) are clinically available for the treatment of epilepsy (2). Around one third of them are sodium channel blockers, showing efficacy in several common forms of epilepsy (3). However, some genetic forms of epilepsy are caused by a loss of voltage-gated sodium channel (VGSC) function, such as Dravet syndrome (4, 5), with a majority of patients being treatment-resistant, even with optimal treatment profiles. Therefore, there is an urgent need to develop more powerful, safer, and longer-lasting therapeutic strategies for treatment-resistant epilepsy, which also provide bidirectional control of VGSC expression.

MicroRNAs (miRNAs) are ~22 nucleotide-long noncoding RNAs that negatively regulate gene expression by binding to complementary sites in the 3' untranslated region (3′ UTR) of target mRNAs (6, 7). MiRNAs are major regulators of gene expression and have been implicated in the pathophysiology of epilepsy (8–11). As miRNAs regulate multiple gene pathways simultaneously (12), they are an attractive target in the treatment of epilepsy where complex and diverse mechanisms give rise to imbalances between excitation and inhibition (13). This includes modulating the expression of voltage-gated ion channels (14, 15). For example, Sosanya et al. reported that miR-129 regulated the expression of *Kcna1*, encoding the voltage-gated potassium channel $K_V1.1$ (16). Inhibition of miR-324 using an antisense oligonucleotide "antimiR" increases protein levels and surface expression of the voltage-gated potassium channel $K_V4.2$, resulting in delayed onset of *status epilepticus* in mice (17), and protecting against spontaneous seizures in the chronic pilocarpine model (18). There is also some evidence that miRNAs influence expression of certain VGSC subtypes (19). Other work suggests that antimiRs can have therapeutic effects in

This article is a PNAS Direct Submission.

[1]G.M. and D.C.H. contributed equally to this work.

[2]To whom correspondence may be addressed. Email: dhenshall@rcsi.ie.

This article contains supporting information online at https://www.pnas.org/lookup/suppl/doi:10.1073/pnas.2216658120/-/DCSupplemental.

Published July 18, 2023.

monogenic neurodevelopmental disorders in which seizures are a comorbidity (20).

There remains a need to identify miRNAs that could be therapeutic targets or biomarkers for common and rare epilepsies. Recent studies have demonstrated that systems approaches that triangulate commonly (dys)regulated miRNAs using miRNA tissue datasets are successful in identifying miRNA targets for epilepsy (10, 21). A complementary strategy could be to search for miRNAs whose expression is altered by administration of effective antiseizure therapies. In this regard, cannabidiol (CBD) has recently been approved for treatment-resistant epilepsies, in particular Dravet syndrome (22, 23), although the mechanism of action remains poorly understood.

Here, we used tissue and biofluid miRNA datasets to identify miR-335-5p and a combination of in vivo seizure models, ex vivo brain slice, and in vitro electrophysiology, molecular biology and in silico analyses to show that miR-335-5p represses a network of genes which includes VGSCs. Correspondingly, bidirectional modulation of miR-335-5p alters seizures in mice. These findings suggest that miR-335-5p modulation may represent a therapeutic strategy for epilepsies and other diseases associated with neuronal excitability.

Results

miRNA Profiling Converges on miR-335-5p. The triangulation of miRNAs commonly dysregulated across diverse datasets has proven an effective strategy to identify miRNAs relevant to treatment-resistant epilepsy (10, 21). However, previous approaches were relatively homogenous, for example, using only rodent model data which lack the variability of human epilepsy. To increase the translational relevance, we explored miRNAs intersecting across datasets with greater heterogeneity and potential relevance to treatment-resistant epilepsy.

To enrich for functional miRNAs, we first generated Argonaute 2 (Ago2) sequencing data for each major hippocampal subfield in a toxin-free model of treatment-resistant temporal lobe epilepsy (TLE) in rats (10). For the chronic epilepsy time point, a total of 79 differently expressed (DE) miRNAs in the dentate gyrus, and 51 and 35 DE miRNAs for CA3 and CA1 respectively were identified, with 15 DE miRNAs common to all hippocampal subfields. This included examples of miRNAs previously linked to epilepsy including miR-146a-5p (24, 25), as well as several miRNAs for which no substantial link to epilepsy has been made previously (Fig. 1*A* and Dataset S1). Next, we looked for miRNAs that were altered upon treatment with CBD, a recently approved ASM for certain treatment-resistant epilepsies (22, 23). A 5-d course of CBD treatment in mice resulted in 66 DE miRNAs in the hippocampus (Fig. 1*A* and Dataset S2). Among these, we detected altered levels of epilepsy-associated miRNAs including lower levels of miR-124-3p and higher levels of miR-132-3p (Dataset S2). Finally, we mined miRNAs dysregulated in plasma samples from video-EEG-monitored patients undergoing presurgical evaluation for focal treatment-resistant epilepsy (26) (Fig. 1*A*).

Intersecting these three datasets was a single miRNA, miR-335-5p (*MIR335* in humans), which was altered in all three hippocampal subfields in the rat Ago2-sequencing dataset, the patient blood samples and after CBD treatment in mice (Fig. 1*A*). Importantly, the mature sequence of miR-335-5p is fully conserved between rodents and humans (*SI Appendix*, Table S1). Expression analysis in the rat model revealed decreased levels of miR-335-5p in the chronic epilepsy phase within all three hippocampal subfields (Fig. 1*B*), as well as after CBD treatment (Fig. 1*C*). In contrast, miR-335-5p levels were elevated in blood samples of treatment-resistant epilepsy patients (Fig. 1*D*). Because the direction of change differed between the rodent brain (down-regulated) and human plasma (up-regulated), we also explored hippocampal miRNA data from patients who underwent resective surgery for treatment-resistant epilepsy. This revealed miR-335-5p was down-regulated, matching the rodent brain findings (*SI Appendix*, Fig. S1 and ref. 27). Interrogation of a miRNA tissue atlas revealed enriched levels of miR-335-5p in the brain compared to other organs (28, 29).

Targets and Cellular Expression of miR-335-5p. To identify the mRNA transcripts regulated by miR-335-5p, we searched experimentally validated [miRTarBase (30) and TarBase (31)] and predicted [miRDiP (32)] miRNA-target interaction (MTI) databases. This identified putative brain-expressed and epilepsy-related mRNA

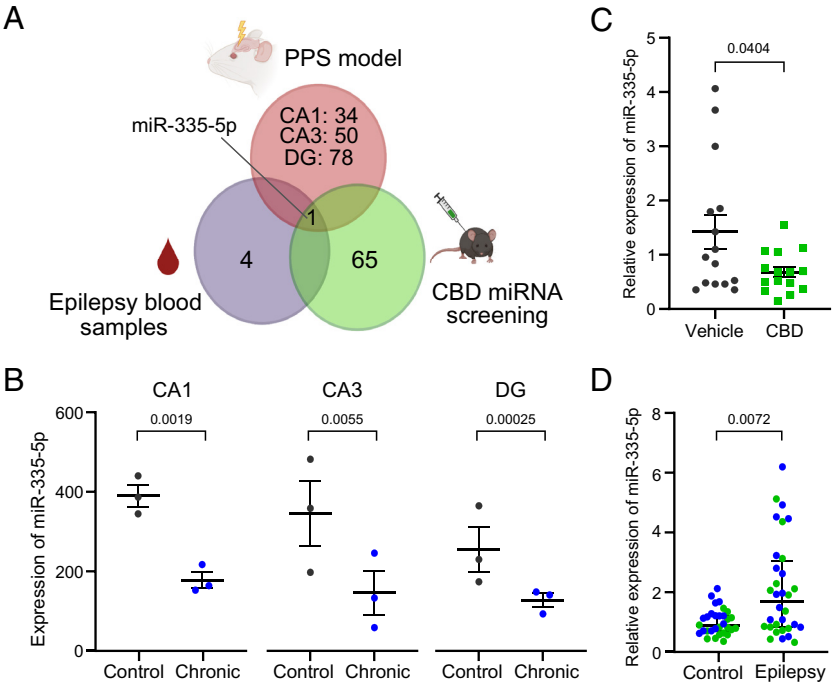

Fig. 1. MiR-335-5p as a common miRNA in experimental and human epilepsy, and in response to CBD. (*A*) MiR-335-5p emerged as the only common miRNA from interrogating tissue and biofluid miRNA datasets from a rodent model and epilepsy patients, and from CBD-treated mice. (*B*) Expression profile of miR-335-5p within the hippocampal circuit of the rodent epilepsy model with lower levels in the chronic epilepsy phase (n = 3/group). CA1: $P = 0.0019$, CA3: $P = 0.0055$, DG: $P = 0.00025$; pairwise comparison using DESeq2. (*C*) Relative expression of miR-335-5p after CBD treatment (n = 15/group). $P = 0.0404$, unpaired *t* test. (*D*) MiR-335-5p plasma levels in treatment-resistant epilepsy patients and control from two different clinical centers (n = 26 to 27/group). Green = samples from hospital in Dublin; blue = samples from hospital in Marburg, see ref. (26). $P = 0.0072$, Mann–Whitney *U* test. CA = cornu ammonis region, CBD = cannabidiol, DG = dentate gyrus, PPS = perforant path stimulation. Graphics in (*A*) were produced using Biorender.

targets of miR-335-5p including genes encoding for several subtypes of VGSCs including *SCN2A* and *SCN3A* (Dataset S3). *SCN1A* was also a likely target of miR-335-5p, with medium confidence [miRDiP (32)]. Pathway enrichment analysis revealed that many of the targets of miR-335-5p are involved in pathways related to neuronal excitability (Fig. 2*A* and Dataset S4).

To extend and validate these insights, we generated a human dataset of RNAs bound to AGO2 by performing individual-nucleotide resolution UV cross-linking and immunoprecipitation (iCLIP) (33) using resected hippocampal samples from treatment-resistant epilepsy patients. This gives an indication of which predicted targets of miR-335-5p are functionally repressed in the RNA-induced silencing complex in human epileptic foci. This analysis revealed 184 transcripts bearing seed targeting sites for miR-335-5p cross-linked to AGO2, including *SCN2A* (Fig. 2*B*). Thus, miR-335-5p actively represses VGSCs in human epilepsy.

We next explored the cell type-specific expression of miR-335-5p. The pathway enrichment analysis of miR-335-5p strongly implicates neuronally expressed targets. To test this idea, we cross-referenced the list of miR-335-5p iCLIP targets with single-cell expression data from the human brain (Allen Brain Atlas – https://portal.brain-map.org/). The transcripts bound to miR-335-5p in human epilepsy were predominantly expressed in excitatory and inhibitory neurons, with few genes identified as of glial origin (Fig. 2*C* and *SI Appendix*, Fig. S2). This strongly indicates that miR-335-5p is functionally active in neurons in human treatment-resistant epilepsy.

In Vivo Modulation of miR-335-5p Alters VGSC Expression and Neuronal Excitability. We hypothesized that if miR-335-5p regulates VGSCs, then inhibiting miR-335-5p should result in upregulation of target expression and produce detectable changes to sodium channel–related electrophysiological properties. To test this, we began by blocking miR-335-5p in the mouse brain using a locked nucleic acid antimiR (Ant-335). Adult C57BL/6 mice received an intracerebroventricular (i.c.v.) microinjection of Ant-335 or a nontargeting scrambled control and then ex vivo brain slices were prepared to determine the biophysical effects of miR-335-5p inhibition (Fig. 3 *A* and *B*). We used current clamp recordings in hippocampal CA1 pyramidal neurons to assess their firing properties. Action potentials of neurons from Ant-335-treated mice had a larger amplitude (Fig. 3 *C* and *D*) and rising slope (Fig. 3 *C* and *F*) compared to controls, but half-width (Fig. 3 *C* and *E*) and decay slope (Fig. 3 *C* and *G*) were unaffected. Ant-335 treatment also increased the maximum firing frequency of pyramidal neurons in response to prolonged depolarization (Fig. 3 *H* and *I* and *SI Appendix*, Figs. S3 and S4). Ant-335 did not alter field response to electrical stimulation, consistent with a relatively specific change in VGSC function (*SI Appendix*, Fig. S5). Correspondingly, we found increased levels of *Scn1a*, *Scn2a*, and *Scn3a* transcripts in mouse hippocampal tissue 48 h after inhibition of miR-335-5p (Fig. 3*J* and *SI Appendix*, Fig. S6). *Scn8a* transcripts were unchanged (Fig. 3*J* and *SI Appendix*, Fig. S6). Furthermore, analysis of an existing microarray dataset (34) shows that several VGSC transcripts, including *SCN1A* and *SCN2A*, are up-regulated in the epileptic human hippocampus (*SI Appendix*, Table S2), consistent with data showing decreased miR-335-5p in such tissue (*SI Appendix*, Fig. S1 and ref. 27).

Inhibition of miR-335-5p Increases VGSCs in Human Induced Pluripotent Stem Cell (iPSC)-Derived Neurons. To validate the mouse findings in a human brain–relevant cellular model, we treated human iPSC-derived neurons (mixed glutamatergic/ GABAergic) differentiated for 4 wk in vitro with either Ant-335 or a nontargeting control for 48 h (Fig. 4*A*). qRT-PCR confirmed Ant-335 potently inhibited miR-335-5p (Fig. 4*B*) and resulted in upregulation of *SCN1A*, *SCN2A*, and *SCN3A* (Fig. 4*C*). We applied a series of test pulses to a range of potentials from −100 mV to 0 mV for 100 ms in 10 mV increments from a holding potential of −110 mV, eliciting fast activating and inactivating inward I_{Na} in neurons (Fig. 4*D*). The current density was calculated at each step pulse and plotted against the holding potential (Fig. 4*E*). Neurons treated with Ant-335 exhibited a significantly larger sodium current density during the 100-ms pulse compared with controls.

Inhibition of miR-335-5p In Vivo Increases Seizure Susceptibility. Both loss- and gain-of-function mutations in several VGSCs can result in an epileptic phenotype (35). We next tested the effects of modulation of miR-335-5p on seizures in vivo. We first explored the effects of miR-335-5p inhibition. Here, we used the pentylenetetrazol (PTZ) model of acute generalized seizures, a common first in vivo screening tool for epilepsy therapies (36) (Fig. 5*A*). qRT-PCR confirmed robust knockdown of miR-335-5p following i.c.v. antimiR injection in mice (Fig. 5*B*). Although mice treated with Ant-335 experienced similar seizure severity to controls given PTZ (Fig. 5*C*), the 45% of Ant-335-treated mice which developed score 5 seizures on the Racine scale (fully developed tonic-clonic seizures) exhibited a shorter latency to tonic-clonic seizures compared to the control group (Fig. 5*D*), consistent with the biophysical and molecular effects of Ant-335 on VGSCs. Furthermore, we observed a positive correlation between miR-335-5p expression and latency to tonic-clonic seizure onset (Fig. 5*E*), suggesting lower levels of miR-335-5p are associated with increased vulnerability to seizures.

To extend these insights, we tested Ant-335 in two additional in vivo models. *Status epilepticus* induced by intra-amygdala kainic acid has higher throughput than the rat PPS model and a defined drug-resistance profile that has been used extensively for antimiR testing (37)(Fig. 5*F*). Consistent with the PTZ model findings, Ant-335-treated mice had reduced time to seizure onset following intra-amygdala kainic acid (Fig. 5*G*). Then, we tested whether Ant-335 could obviate the antiseizure effects of CBD in the PTZ model (38) (Fig. 5*H*). Dosing mice with CBD reduced the severity of PTZ-induced seizures, and this protective effect was partly reversed in animals treated with Ant-335 (Fig. 5*I*).

Seizure Suppressive Effects of AAV-Delivered miR-335-5p. To explore whether overexpression of miR-335-5p might have antiseizure effects, we used a viral vector-based approach, using an adeno-associated virus (AAV) serotype 9 expressing the pri-miR-335 sequence driven by a human synapsin (hSYN) promoter (AAV9-miR-335). AAV9-miR-335 or a scrambled version (AAV9-Scr) were injected bilaterally into the ventral hippocampi (Fig. 6 *A* and *B*). After 2 wk, we detected ~10-fold to 16-fold upregulation of miR-335-5p in the ventral hippocampus of AAV9-miR-335 mice compared to animals given the vector containing the scrambled sequence (Fig. 6*C*). MiR-335-5p was also overexpressed in the dorsal hippocampus of AAV9-miR-335 mice, presumably due to spread of the virus from the injection site (*SI Appendix*, Fig. S7). Crucially, both AAV9-miR-335 and Ant-335 did not affect the expression of several other brain-enriched miRNAs, confirming minimal off-target effects of this approach (*SI Appendix*, Fig. S8).

To assess whether miR-335-5p upregulation had antiseizure effects, we tested mice using the PTZ model. Overexpression of miR-335-5p resulted in lower seizure severity, with only 16% of AAV9-miR-335-treated mice developing tonic-clonic seizures after PTZ compared to over 60% in the AAV-Scr group (Fig. 6*D*). For those mice which did experience tonic-clonic seizures, no clear

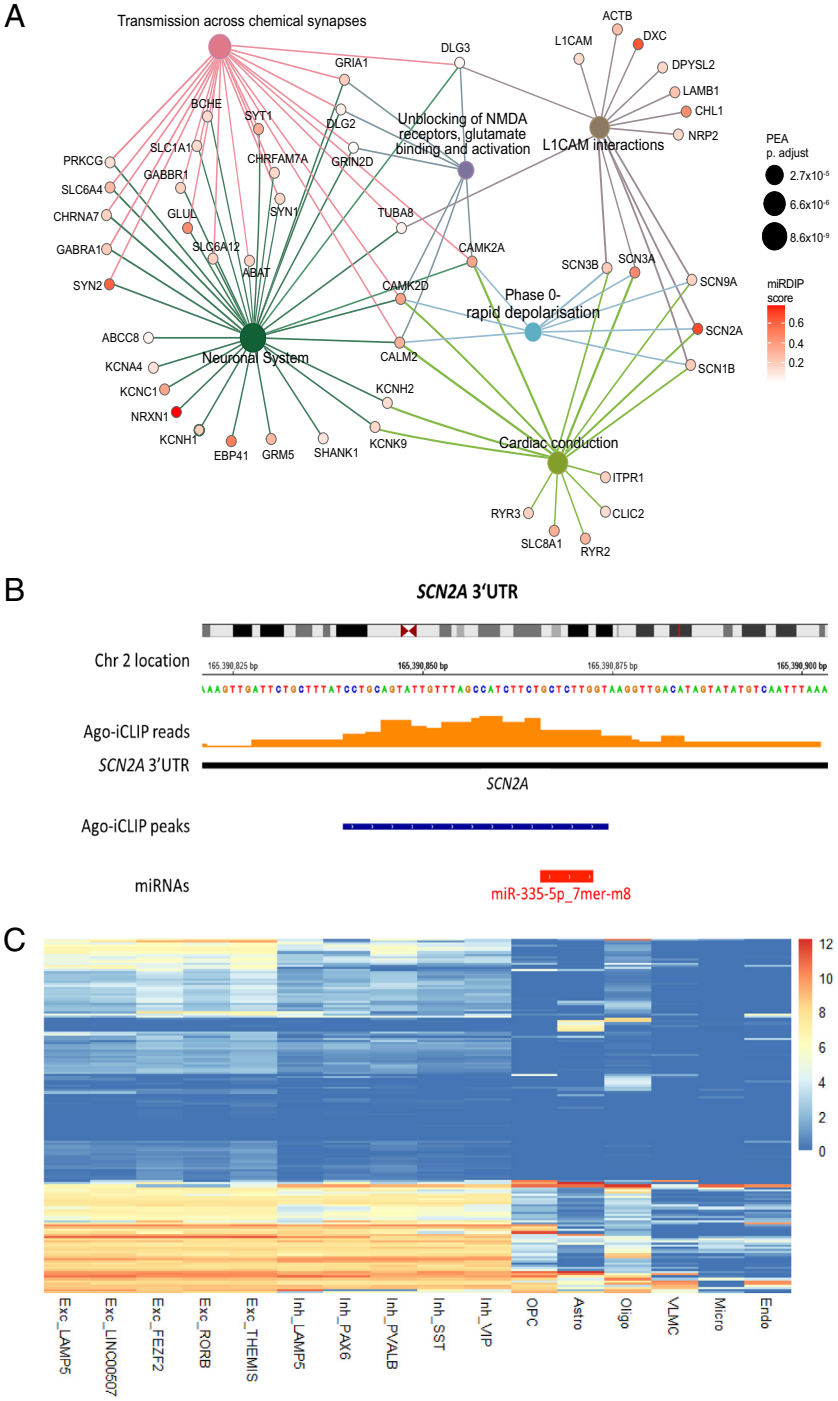

Fig. 2. Targets of miR-335-5p are predominately expressed in neurons and play an important role in pathways of neuronal excitability. (*A*) Top six significantly enriched Reactome pathways (sized according to p-value) from pathway enrichment analysis of the mRNA targets of miR-335-5p (miR-335-5p targets from target identification pipeline). The miR-335-5p mRNA targets associated with each pathway are colored according to miRDiP integrated score (*Materials and Methods*). Links between pathways and mRNA nodes are colored according to the pathway. (*B*) iCLIP data from human epilepsy patients identified that the *SCN2A* gene, which is located in chromosome 2, encodes a transcript with a target site for miR-335-5p. The orange bars represent the aggregated iCLIP reads across all the patient samples that map along the *SCN2A* gene. (*C*) Heatmap of the expression levels of miR-335-5p iCLIP targets across different cell types in the human primary motor cortex. Values are shown as trimmed means of Log_2(CPM+1)(CPM = Counts Per Million). (Trimmed mean = average expression of the middle 50% of the data for each gene and cell type). Exc = Excitatory Neurons, Inh = Inhibitory Neurons, OPC = Oligodendrocyte Precursor Cells, Astro = Astrocytes, Oligo = Oligodendrocytes, VLMC = Vascular Leptomeningeal Cells, Micro = Microglia, Endo = Endothelial Cells. Excitatory and inhibitory neurons are further divided in subtypes according to the expression of the specified marker genes. Data were sourced from the Allen Brain Atlas (https://portal.brain-map.org/).

change in the latency to tonic-clonic seizures was observed after miR-335-5p overexpression (Fig. 6*E*); however, statistical comparison was not possible as only two AAV9-miR-335 treated mice reached this stage. Antiseizure effects were also reflected in the higher survival rate of mice overexpressing miR-335-5p compared to controls (Fig. 6*F*). After, we extracted brain samples from the mice for molecular analysis of the AAV9 injection site in the ventral hippocampal region. Individual animals displayed variation in levels of miR-335-5p and VGSCs. However, we observed the expected anticorrelation between miR-335-5p and VGSC transcripts in most samples. That is, mice treated with AAV9-miR-335 had lower levels of several VGSC subtypes, with the highest reduction observed for *Scn1a,* whereas mice treated with the scrambled sequence typically displayed higher levels of VGSC transcripts (Fig. 6*G* and *SI Appendix*, Fig. S9). We did not detect protective effects of AAV9-miR-335 against seizures evoked by intra-amygdala kainic acid (*SI Appendix*, Fig. S10). Finally, we explored animal behavior in AAV9-treated mice. AAV9-miR-335 mice performed similarly to AAV-Scr-treated animals in tests of cognition and naturalistic behavior, including the open field, Y-maze, marble burying, and nest building (*SI Appendix*, Figs. S11 and S12).

Discussion

The present study used model-based, drug-altered and human epilepsy biomarker datasets to search for miRNAs regulating neuronal excitability via mechanisms relevant to seizure control. Triangulation converged on miR-335-5p, a brain-enriched

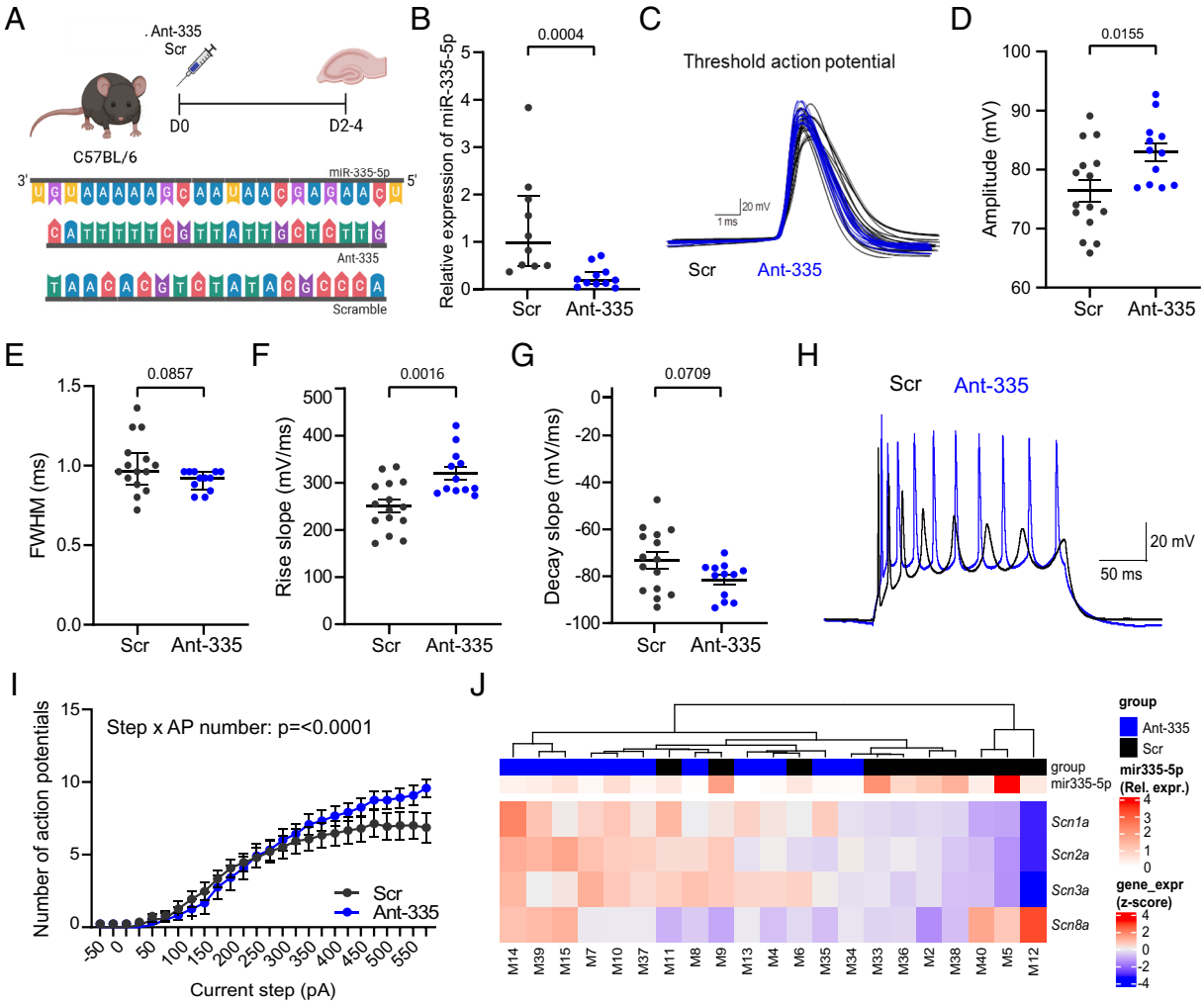

Fig. 3. Effect of miR-335-5p inhibition on hippocampal biophysics and expression of voltage-gated sodium channel in naïve mice. (*A*) Schematic shows the experimental design. Briefly, adult mice were injected i.c.v. with either Ant-335 or a scrambled (Scr) sequence (sequences shown below schematic) and brain slices were prepared after 2 to 4 d for ex vivo electrophysiology. (*B*) Relative expression of miR-335-5p measured 48 h after i.c.v. injection of Ant-335 or scramble. $P = 0.0004$, Mann–Whitney *U* test. (*C*) Overlay of the threshold action potentials obtained from Ant-335- (blue) and scramble- (black) treated hippocampal CA1 pyramidal neurons. (*D*) Ant-335 increased action potential amplitude. $P = 0.0155$, unpaired *t* test. (*E*) Action potential full-width half maximum (FWHM) was not changed after Ant-335 treatment. $P = 0.0857$, Mann–Whitney *U* test. (*F*) The rising phase was characterized by a larger rise slope in Ant-335 treated neurons. $P = 0.0016$, unpaired *t* test. (*G*) Decay slope was not altered. $P = 0.0709$, unpaired *t* test. (*H*) Representative raw traces from Ant-335- (blue) and scramble- (black) treated neurons. (*I*) Ant-335 increased the maximum firing frequency of pyramidal neurons, which were able to fire above the plateau seen in control neurons, $P <= 0.0001$, two-way repeated measures ANOVA) Electrophysiology: n = 12 to 15 neurons per group. (*J*) Heatmap showing relative mRNA expression of the various VGSCs in the hippocampus after i.c.v. injection of Ant-335 or Scr (n = 10 to 11/group, mRNA expression levels (gene_expr) are z-score normalized). Expression levels of miR-335-5p [from (*B*)] of the corresponding animals are also shown to observe links between expression levels of miR-335-5p and expression of VGSCs. Correction for multiple comparisons was applied on electrophysiological data and α was adjusted to 0.01. Graphics in (*A*) were produced using Biorender.

miRNA (28, 29). This complements similar approaches which yielded additional miRNA targets for epilepsy (21, 39), but here we used exclusively profiling data rather than one or more prediction-based strategy. Notably, miR-335-5p did not appear as a leading candidate miRNA when only animal model miRNA profiles were screened (10, 40). This supports the benefits of including human data and more divergent rather than homogenous data sources of miRNA profiling for the identification of miRNA targets, an approach that may have value for other brain diseases. Meta-analysis of miRNA epilepsy datasets has previously identified miR-335-5p (40, 41) (*SI Appendix*, Table S3). Notably, levels of miR-335-5p appear to vary between models, consistent with temporally- and activity-controlled miRNA expression. While we found lower levels of miR-335-5p in the three subfields of the hippocampus of rats that developed TLE, miR-335-5p upregulation has been reported in the hippocampus in some models (27, 42, 43), as well as downregulation (41, 44, 45). Levels of miR-335-5p were also down-regulated in resected hippocampal tissue from patients with TLE and hippocampal sclerosis (27). Since miR-335-5p is likely neuron-enriched, based on the single-cell expression profiles of its targets, this reduction may reflect neuronal loss, variation in which might also explain inconsistencies in levels of miR-335-5p-regulated VGSCs among rodent and human studies (34). In contrast, plasma levels of miR-335-5p were higher in treatment-resistant epilepsy patients (26). This could reflect passive or active transfer of miR-335-5p, from sites of damage or seizure onset within the brain to the blood, perhaps AGO2-bound or exosome-enclosed. Bidirectional brain-blood miRNA profiles have been reported for other neuronal miRNAs in epilepsy and blood levels of brain-expressed miRNAs rise after seizures in refractory epilepsy patients (46–48). The availability of models to track the movement of brain-enriched miRNAs to the circulation may enable mechanistic understanding of the transfer process (49).

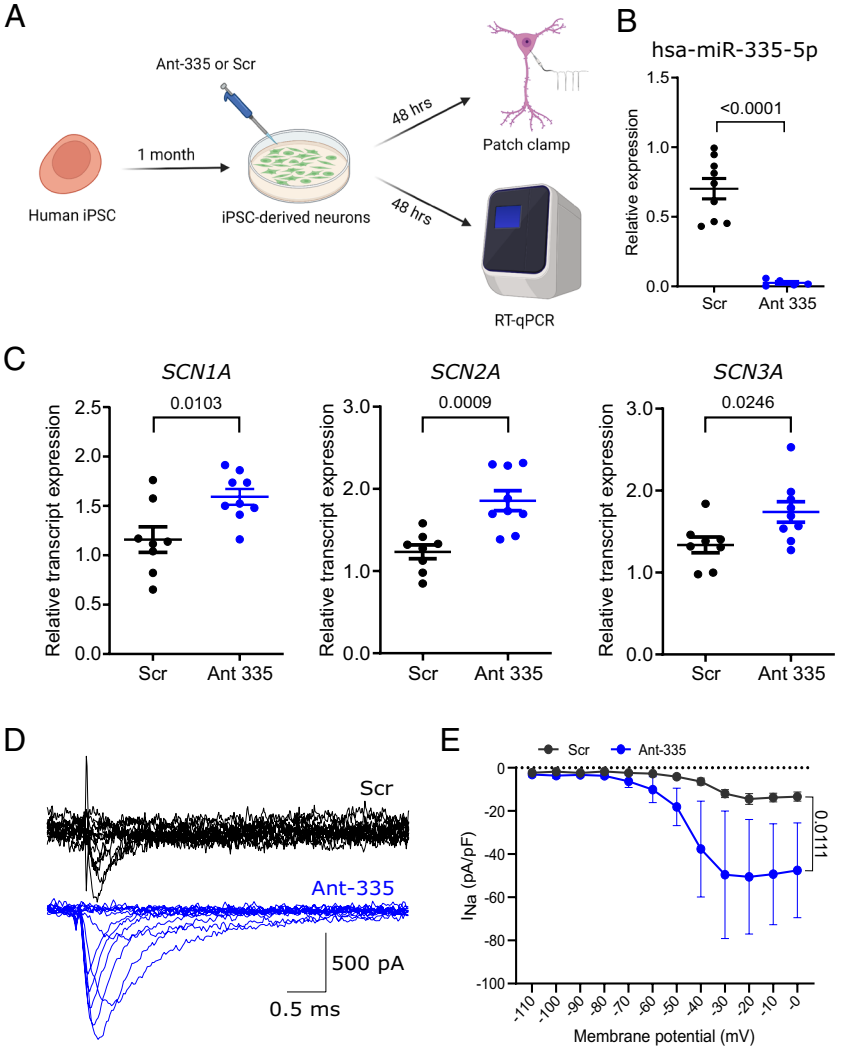

Fig. 4. Effect of miR-335-5p inhibition on voltage-gated sodium currents in iPSC-derived neurons. (*A*) Schematic shows the experimental design. Human iPSC-derived neurons were differentiated for 4 wk and treated for 48 h with Ant-335 or scramble (Scr). Voltage-gated sodium currents were then recorded in voltage-clamp mode from transfected neurons. (*B*) qRT-PCR performed on separate iPSC-derived neurons confirmed robust inhibition of miR-335-5p and (*C*) corresponding de-repression of VGSC transcripts. MiR-335-5p: $P = <0.0001$, unpaired *t* test; *SCN1A*: $P = 0.0103$, unpaired *t* test; *SCN2A*: $P = 0.0009$, unpaired *t* test; *SCN3A*: $P = 0.0246$, unpaired *t* test. N = 8 to 9/group. (*D*) Representative traces of voltage-gated sodium current elicited by step depolarizations ranging from −100 mV to 0 mV in 10 mV increments for 100 ms from a holding potential of −110 mV. (*E*) Current density curve showing the peak current density at different holding potentials (n = 6 to 8 neurons). $P = 0.0111$, two-way repeated measures ANOVA. Graphics in (*A*) were produced using Biorender.

The present study used a combination of AAV- and antimiR-based approaches to evaluate the actions of miR-335-5p on neuronal excitability. This complements other genetic on-off modulation of miRNAs (21, 50), and provides stronger evidence than single-direction manipulations that use knockdown or overexpression alone. Using the PTZ model to evoke generalized seizures, we found that upregulation of miR-335-5p reduces seizure severity whereas reducing miR-335-5p levels produced opposite results, increasing seizure susceptibility. This indicates miR-335-5p plays a functional role in the fine control or adjustment of neuronal excitability and is an additional miRNA target to explore as an approach to the treatment of epilepsy.

Here, we provide evidence that VGSCs may be key targets of miR-335-5p and underlie the seizure-regulating effects of altered miR-335-5p expression, although we did not demonstrate whether this is direct (via 3′UTR targeting) or indirect (e.g., via secondary or compensatory changes). Inhibition of miR-335-5p increased levels of at least three VGSC transcripts in mice and increased pyramidal neuron excitability, as indicated by enhanced depolarization and firing frequency. The biophysical changes suggest a relatively specific effect on functional VGSC expression, as these channels underlie the rising phase of the action potential (51). Increased voltage-gated sodium currents and VGSC transcripts were validated in human iPSC–derived neurons, indicating translational potential. This is further supported by the fully conserved sequence of miR-335-5p, and its interaction with *SCN2A* in the human brain (*SI Appendix*, Fig. S13), a consideration in preclinical development of miRNA-based therapies (37). The key VGSCs in mature pyramidal neurons are encoded by *Scn2a* and *Scn8a* (52) and, intriguingly, our study revealed that *Scn2a*, but not *Scn8a*, was increased by Ant-335. Furthermore, *Scn2a* was among the targets predicted with high confidence in our miR-335-5p target identification pipeline. The changes mediated by miR-335-5p inhibition, observed especially in the rising phase, might be largely driven by modulation of *Scn2a*. Besides changes in *Scn2a* expression, we also observed an upregulation of *Scn1a* and *Scn3a* after miR-335-5p inhibition, suggesting that miR-335-5p also has the potential to shape the activity of inhibitory interneurons, which predominantly use these VGSC subtypes (52, 53). We note that despite miR-335-5p dysregulation in the PPS model, we did not see an associated change in VGSC transcripts in the chronic phase (*SI Appendix*, Table S4). This may be due to other compensatory molecular mechanisms, or reduced signal following neuronal loss.

Modulating VGSC function provides potent but context-specific seizure control. In common forms of treatment-resistant epilepsy, including TLE and gain-of-function sodium channelopathies, sodium channel blockers are highly effective (3, 54). Reduced VGSC function, for example in Dravet syndrome, instead requires augmentation of sodium currents, probably in specific cell types. The bidirectional effect of miR-335-5p on excitability can be exploited, therefore, delivering miR-335-5p for certain forms of epilepsy which respond to sodium channel blockers, whereas for

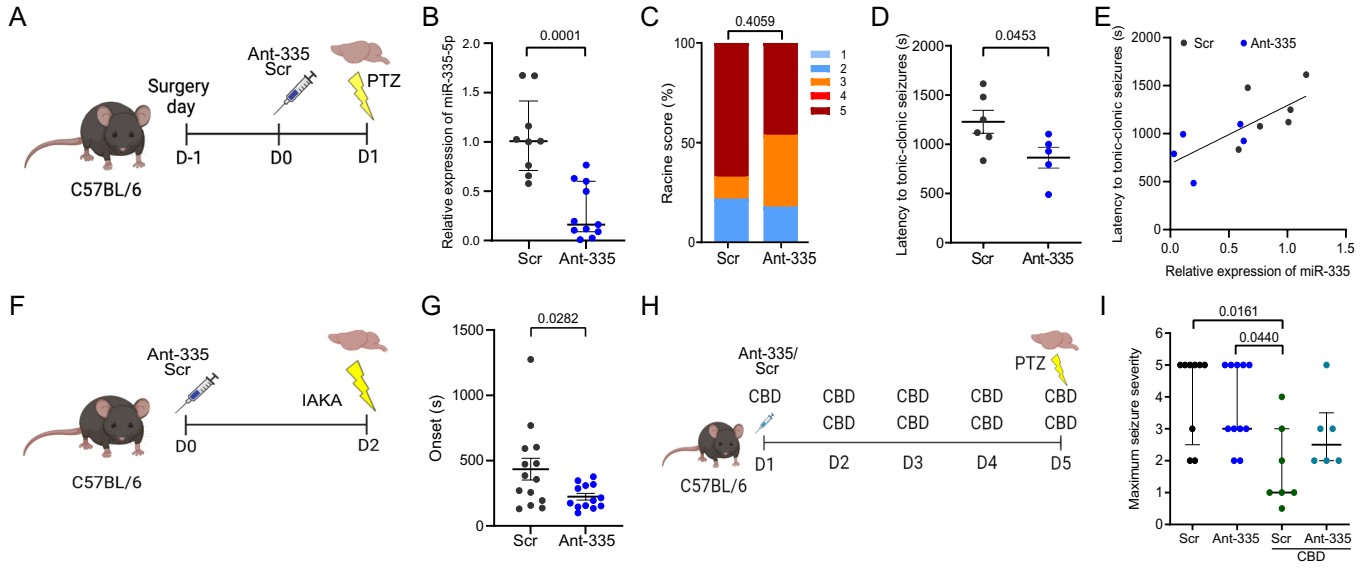

Fig. 5. miR-335-5p inhibition increases seizure susceptibility in mouse models. (*A*) Schematic shows the experimental design for PTZ testing. Mice were equipped with a guide cannula and injected i.c.v. with either Ant-335 or a scrambled sequence. Seizures were induced 24 h after the treatment via an i.p. injection of PTZ (80 mg/kg). (*B*) Relative expression of miR-335-5p measured 24 h after i.c.v. injection of Ant-335 or scramble (n = 9 to 11/group). $P = 0.0001$, Mann–Whitney U test. (*C*) Racine scale scores assessed seizure severity in the two groups (n = 9 to 11/group). $P = 0.4059$, Fisher's exact test. (*D*) Latency to tonic-clonic seizures was decreased in animals treated with Ant-335 which reached Racine scale 5. $P = 0.0453$, unpaired t test. (*E*) Positive correlation between miR-335-5p expression and latency to tonic-clonic seizures. r = 0.7230, $R^2 = 0.5228$, $P = 0.0119$. (*F*) Experimental design for intra-amygdala kainic acid (IAKA) testing. (*G*) Ant-335 reduced the time to onset of *status epilepticus* (SE) following IAKA (n = 13 to 14/group). $P = 0.0282$, unpaired t test. (*H*) Experimental design to test the impact of Ant-335 on seizure susceptibility in CBD-treated mice. (*I*) Ant-335 counteracts the reduction in seizure severity observed with CBD treatment (n = 7 to 11/group). The Kruskal–Wallis test with Dunn's multiple comparisons test. Graphics in (*A*, *F*, and *H*) were produced using Biorender.

Dravet syndrome or other loss-of-function sodium channelopathies, the antimiR would enable potential restoration of VGSC function. While the PTZ model is well suited to proof-of-concept studies of seizure modulators, screening through additional models of drug resistance will be needed. Indeed, the strength of antiseizure effect produced by AAV-miR-335 was not as strong as observed after CBD (38) or for other traditional ASMs such as carbamazepine and sodium valproate (55, 56). We also observed no effect of AAV9-miR-335 on seizure onset in the intra-amygdala kainic acid model. An AAV approach would, however, offer a means of prolonged control of VGSC function versus frequent, daily dosing with traditional ASMs and would also offer opportunities to target specific cell types. For example, overexpressing miR-335-5p in excitatory neurons could preserve the excitability of interneurons and produce more potent seizure-suppressive effects. Future studies could explore strategies that restrict miR-335-5p to specific cell types. Similarly, target site blockers could be used to interfere with miR-335-5p effects on single sodium channel transcripts (57). This could avoid the pro-excitability effects of broad miR-335-5p suppression by antimiRs while enabling upregulation of single transcripts, an approach that could have utility for the treatment of Dravet syndrome in which the *Scn1a* transcript is haploinsufficient (58, 59).

Although our results indicate an important interaction between miR-335-5p and VGSCs, our iCLIP analysis predicts more than one hundred mRNA targets of miR-335-5p. This includes transcripts encoding ionotropic and metabotropic glutamate receptors and potassium channels. Our electrophysiological data were not, however, consistent with functional changes in these targets. For example, we did not observe changes in population synaptic activity or neuronal repolarization, which suggests that miR-335-5p's interaction with these targets is less important for the major effects we observed. Importantly, behavioral testing did not indicate any adverse impact of overexpressing miR-335 on cognitive function or naturalistic behaviors. Taken together, the combination of functional, molecular, biophysical, and behavioral approaches in vivo, ex vivo, and in silico favors the effect of modulating miR-335-5p involving altered expression of VGSCs.

The present study provides important datasets on the functional targets of miRNAs in the human hippocampus, subfield-specific miRNA changes in a toxin-free model of epilepsy, and miRNA changes produced by CBD, a recently approved ASM. The iCLIP dataset enables the identification of most targets of miRNAs in a brain structure relevant to treatment-resistant epilepsy. A caveat is the absence of a control human hippocampal dataset to compare to, the generation of which will require technical advances in retaining AGO2:RNA interactions postmortem. An unexpected finding in the present study was that repeated dosing of mice with CBD lowered miR-335-5p levels in the hippocampus. Based on our antimiR studies, this would be expected to increase neuronal excitability. It is likely, therefore, that chronic treatment with CBD elicits homeostatic mechanisms to restore normal neuronal excitability. Interestingly, we observed a slight increase in the expression of *Scn1a*, but not *Scn2a* or *Scn3a*, in CBD-treated mice (*SI Appendix*, Fig. S14). Therefore, there are likely other molecular mechanisms, including other miRNAs, which add further complexity to VGSC regulation, beyond the influence of miR-335-5p. In support of this idea, levels of miR-132, an activity-regulated miRNA have been reported to be higher in CBD-treated mice (60, 61). The findings may help explain why CBD is only effective in certain forms of epilepsy.

Modulating miR-335-5p in vivo may have therapeutic effects beyond seizure control. Capitano et al. showed that training of mice in a spatial memory task–induced downregulation of miR-335-5p in the hippocampus (62). Such paradigms are relevant to synaptic plasticity in the hippocampus. In contrast, overexpression of miR-335-5p impaired spatial memory in the same study. Neuroprotective effects of miR-335-5p have also been reported in some stroke models (63). Further studies are required to determine whether targeting miR-335-5p may impact cognitive or other comorbidities in the setting of epilepsy.

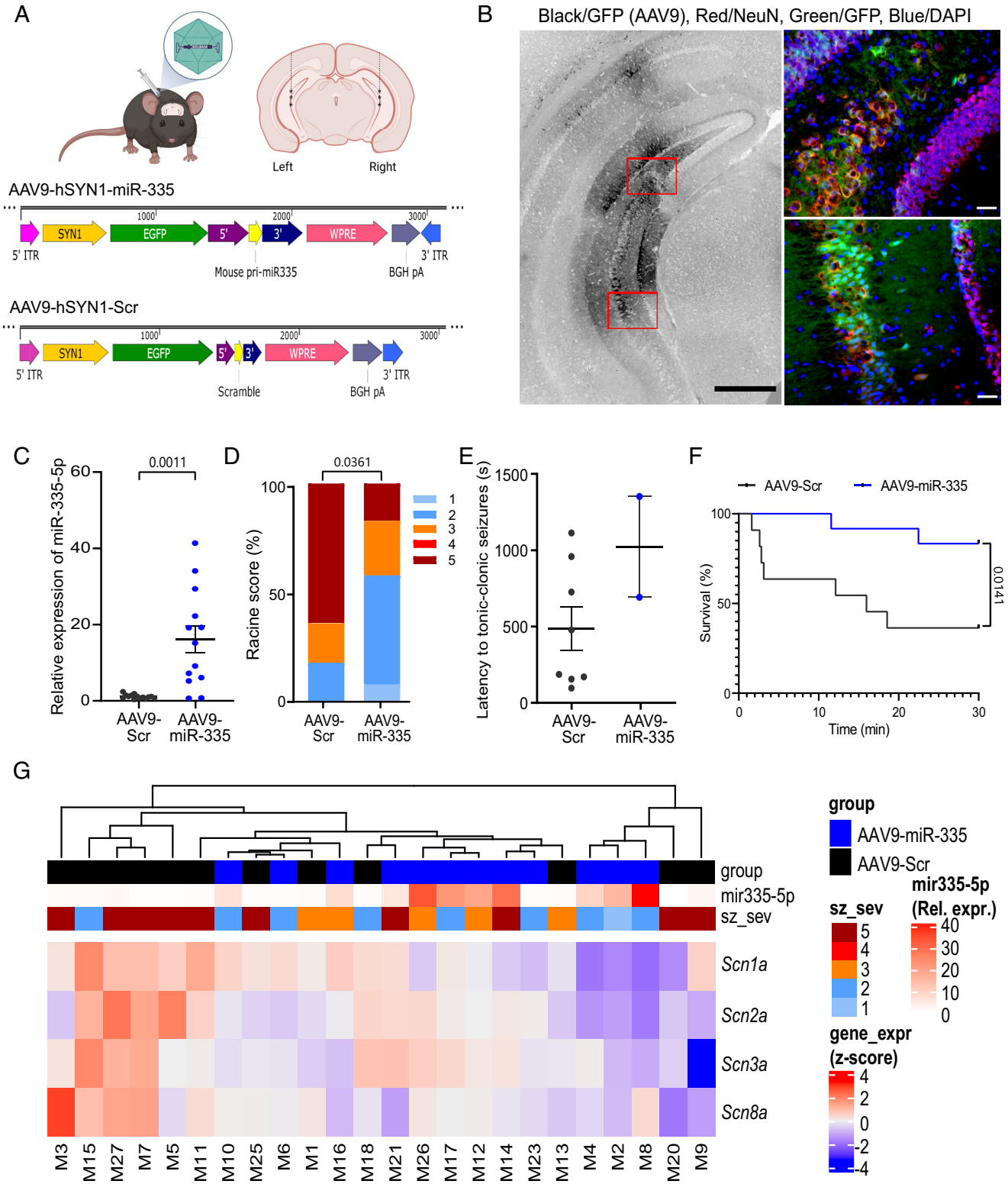

Fig. 6. Effects of miR-335-5p overexpression on PTZ-induced seizures. (*A*) Schematic shows the experimental design. Briefly, adult C57 mice were injected intra-hippocampally with either an AAV9 containing the pri-miRNA sequence of miR-335-5p or a scrambled sequence. Seizures were induced 2 wk after the treatment via an i.p. injection of PTZ (75 mg/kg). (*B*) Expression of AAV9 (black) in the ventral part of the hippocampus. (Scale bar magnification: 500 µm.) Sections marked in red are shown in the small panels besides showing the expression of AAV9 in CA3 pyramidal neurons. NeuN = red, GFP (AAV9) = green, DAPI = blue. (Scale bar magnifications: 50 µm.) (*C*) Relative expression of miR-335-5p in the ventral hippocampus after intra-hippocampal injection of AAV9-miR-335 or control AAV9 (n = 9/group). *P* = 0.0011, unpaired *t* test. (*D*) Racine's scale scores assessed seizure severity in the two groups (n = 11 to 12/group). *P* = 0.0361, Fisher's exact test. (*E*) Latency to tonic-clonic seizures was not affected by the overexpression of miR-335-5p. (*F*) Kaplan–Meier survival analysis for the two different treatment groups. AAV9-Scr group showed a survival rate of 36% whereas animals overexpressing miR-335-5p had a survival rate of 83.3%. *P* = 0.0141, Mantel-Cox test. (*G*) Heatmap showing relative mRNA expression of the various VGSCs in the ventral hippocampus after intra-hippocampal injection of AAV9-miR-335 or control AAV9 [n = 12 per group, mRNA expression levels (gene_expr) are z-score normalized]. Seizure severity scores (sz_sev) and relative expression levels of miR-335-5p are also shown. Levels of miR-335-5p (from *C*) and seizure severity (from *D*) of the corresponding animals were incorporated to observe links between expression levels of miR-335-5p, seizure severity and expression of VGSCs. Graphics in (*A*) were produced using Biorender.

Taking our observations together, miR-335-5p seems to act as an endogenous homeostatic controller of neuronal excitability. Increased neuronal excitability (for example in epilepsy and seizures) may induce the upregulation of miR-335-5p, which in turn protects against excessive excitability in the brain, at least in part through VGSC repression, forming a regulatory feedback loop. There is evidence that miR-335-5p can form a regulatory loop with glutamate receptor, metabotropic 4 (*GRM4*) (64), suggesting that miR-335-5p has similar interactions with other molecular targets linked to neuronal network excitability. Further studies are needed to gain a full understanding of the cellular function of miR-335-5p. Moreover, while we used male mice for in vivo studies, our iPSC studies used cells from a female donor. Thus, it is likely that miR-335-5p modulation will be effective regardless of sex although further study is required.

In conclusion, the present results indicate that miR-335-5p has a role in homeostatic maintenance of neuronal excitability, including via regulation of VGSCs. Modulation of miR-335-5p might be a compensatory mechanism in the brain to counteract neuronal excitability in a bidirectional manner. This could provide an approach to modulating brain activity, with possible therapeutic applications in epilepsy and other neurological diseases.

Materials and Methods

Animal Models of Epilepsy. All experimental procedures involving animals were carried out in accordance with the European Communities Council Directive (2010/63/EU). All animals were housed on a 12 h light–dark cycle under controlled conditions (temperature: 20 to 25 °C; humidity: 40 to 60%). Food and water were available ad libitum.

Procedures on rats were performed in accordance with the local regulation authority (Philipps University Marburg, Germany: Regierungspräsidium Giessen, 73/2013). The PPS model of TLE was performed as previously described (10) and as detailed in *SI Appendix*, using adult male Sprague-Dawley rats (325 to 350 g, Charles River). Briefly, stimulation electrodes were implanted bilaterally into the angular bundle of the perforant path. After surgery, animals were allowed to recover for 1 wk before PPS was applied for 30 min on 2 consecutive days and 8 h on the third day by continuous, bilateral 2-Hz paired-pulse stimuli, with a 40-ms interpulse interval, plus a 10-s train of 20-Hz single-pulse stimuli delivered once per minute. Video and EEG were recorded continuously up to 3 mo. Rats were transcardially perfused with 0.9% NaCl solution 1 mo after first spontaneous seizure (chronic epilepsy). Hippocampi were removed, dissected into the different hippocampal subfields, dentate gyrus, CA1 and CA3 region, and processed for Ago2-sequencing.

Procedures using adult male C57BL/6JOlaHsd mice (25 to 30 g, Harlan) were approved by the Research Ethics Committee (REC 1587) of the RCSI University of Medicine and Health Sciences, under license from the Ireland Health Products Regulatory Authority (AE19127/P057). For the PTZ model, mice received a convulsant dose of 75 to 80 mg/kg (i.p.) PTZ in 0.9% (w/v) NaCl, were video monitored for 30 min, and then transcardially perfused with phosphate-buffered saline (PBS) for tissue sampling (under pentobarbital anesthesia). Videos of PTZ-induced seizures were analyzed offline using a modified Racine scale: 0, no change in behavior; 0.5, abnormal behavior; 1, isolated myoclonic jerks; 2, atypical clonic seizure; 3, fully developed bilateral forelimb clonus; 4, tonic-clonic seizures with suppressed tonic phase with loss of righting reflex; 5, fully developed tonic-clonic seizure with loss of righting reflex (65, 66). Animals which did not present any signs of seizures were excluded from the analysis.

The acute intra-amygdala kainic acid model was performed as detailed previously (10) and in *SI Appendix*. Briefly, mice were equipped with three skull-mounted EEG recording screws (Bilaney Consultants Ltd.) and a guide cannula (coordinates from adjusted Bregma: A/P = −0.95 mm; L = −2.85 mm). For the induction of *status epilepticus*, we used tethered EEG recording to acquire a baseline, before animals were injected with kainic acid (0.3 μg/0.2 μL in PBS; Sigma-Aldrich, Ireland) into the basolateral amygdala. After 40 min, all mice received an i.p. injection of lorazepam (8 mg/kg; Pfizer). EEG data were analyzed and quantified using LabChart 8 Reader (AD Instruments) and MATLAB (vR2020a; MathWorks Inc.), as detailed further in *SI Appendix*.

Drug Administrations. Anesthesia and analgesia were as described in *SI Appendix* for the intra-amygdala kainic acid model. For i.c.v. antimiR administration, a burr hole was drilled above the right lateral ventricle (coordinates from Bregma: A/P = +0.3 mm; L = −0.9 mm; D/V = −2 mm). Mice received either miRCURY LNA power inhibitor for mmu-miR-335-5p (Ant-335; sequence: 5′-CATTTTTCGTTATTGCTCTTG-3′; Qiagen, Cat No.: 339132; 0.1 nmol in 2 μL PBS), or a nontargeting scrambled control (Scr; sequence: 5′-TAACACGTCTATACGCCCA-3; Qiagen, Cat No.: 339137; 0.1 nmol in 2 μL PBS), at a rate of 1 μL/min. The needle was left in place for 5 min after the injection. AntimiR-treated mice were left for 1 to 4 d before further experiments to ensure the maximal silencing (11).

For overexpression of mmu-miRNA-335-5p, AAV9 viral particles expressing mmu-pri-miRNA-335 or a scramble sequence were used. AAV9-SYN1-EGFP-mmu-miR-335-5p (AAV9-miR-335, 4.01×10^{13} GC/mL) or AAV9-SYN1-EGFP-Scramble (AAV9-Scr, 1.09×10^{13} GC/mL) were purchased from VectorBuilder Inc. Vectors were delivered bilaterally into the ventral hippocampus at three different depths (coordinates from Bregma: A/P = −3 mm; L = ±2.62 mm; D/V: −2.5/−3/−3.5 mm from pia). Injections were administered at a rate of 0.1 μL/min, and 0.2 μL was injected per injection site. The needle was left in place for 2 min after each injection. AAV9-treated mice were used for further experiments 2 wk postinjection (67).

CBD (donated by STI Pharmaceuticals Ltd., and PureForm Global Inc.) in a vehicle of 100% ethanol, Kolliphor EL, and 0.9% (w/v) NaCl (2:1:17; all Sigma-Aldrich) was administered twice daily over 5 d via intraperitoneal (i.p.) injections at 200 mg/kg/d. Animals receiving a volume-matched dose of vehicle served as a control. In the combined Ant-335-CBD study, the first CBD injection was replaced with the injection of the antimiR.

Analysis of miRNA Expression. RNA was extracted as described previously (10) and in *SI Appendix*. Two hundred fifty nanogram RNA was reversed transcribed using stem-loop Multiplex primer pools (Applied Biosystems). Reverse-transcriptase-specific primers for mmu-miR-335-5p (Applied Biosystems miRNA assay ID 000546), mmu-miR-134-5p (ID 001186), mmu-miR-22-3p (ID 000398), mmu-miR-132-3p (ID 000457), and mmu-miR146a-5p (ID 000468) were used and real-time quantitative PCR performed using TaqMan miRNA assays (Applied Biosystems) on the QuantStudio™ Flex PCR system (Thermo Fisher Scientific). Comparative CT values were measured. MiRNA levels were normalized using U6B (Applied Biosystems miRNA assay ID 001093) or RNU19 (Applied Biosystems miRNA assay ID 001003) expression, and relative fold change in miRNA levels were calculated using the comparative cycle threshold method ($2^{-\Delta\Delta CT}$). Ago2 immunoprecipitation and small RNA sequencing methods are as described previously (10) and are detailed in *SI Appendix*.

Analysis of Individual mRNA Expression. Five hundred fifty nanogram RNA was reversed transcribed into cDNA using Superscript II Reverse Transcriptase enzyme. qRT-PCR was performed on a LightCycler 1.5 (Roche diagnostics Ltd.) using the QuantiTech SYBR Green PCR kit (Qiagen Ltd.). Transcript levels were normalized to *β-actin* and relative fold change calculated using the comparative cycle threshold method ($2^{-\Delta\Delta CT}$). Primers are listed in *SI Appendix*, Table S5. Heatmaps of mRNA expression were generated using the ComplexHeatmap package in R (68).

MTI Identification and Pathway Enrichment Analysis. We first verified that the sequence of miR-335-5p is conserved across humans and mice (miRBase V22) (69). Predicted mRNA targets of hsa-miR-335-5p were identified using miRDiP V4.1. (32). Experimentally validated MTIs of both hsa-miR-335-5p and mmu-miR-335-5p were obtained from miRTarbase V7 (30) and TarBase V8 (31). Predicted MTIs with no experimental evidence were retained only if they were classed as "Very High" confidence by miRDiP. MTIs were retained if the mRNA targets are expressed in the brain Atlas (www.proteinatlas.org, downloaded May 13th 2021) (70) and have previously been associated with epilepsy [in-house database collecting information from CARPEDB (http://carpedb.ua.edu), epiGAD (71), Wang et al. (72), and curated epilepsy genes from the Comparative Toxicogenomics Database (CTD; ref. 73). Pathway enrichment analysis of the remaining 267 MTIs (Dataset S3) was performed using the ReactomePA (74) and clusterProfiler (75) packages, with an adjusted p-value (Benjamini–Hochberg) <0.05 considered significant (Dataset S4). All analyses were performed in RStudio (Rversion 4.1.3) (76) using the httr, dplyr, tidyr, and plyr packages (77).

Immunohistochemistry. AAV9-injected mice were perfused with PBS, brains post-fixed in 4% paraformaldehyde, sectioned (12 µm coronal) on a cryostat (CM1900, Leica), and mounted on glass slides. Sections were blocked in 1% BSA for 1.5 h followed by incubation overnight with the primary antibody against NeuN (Millipore). On the next day, slices were washed and then incubated with fluorescent secondary antibody (Invitrogen) for 2 h. Then, sections were rinsed again, stained with DAPI, and mounted and imaged using a Leica DM4000 epi-fluorescence microscope.

Ex Vivo Electrophysiological Recordings. Mouse brain slices were prepared 2 to 4 d after antimiR injection to ensure the maximal miRNA inhibition (11). Mice were killed by sodium pentobarbital overdose (Dolethal, Vetoqinol), transcardially perfused with ice-cold oxygenated sucrose artificial cerebrospinal fluid (ACSF) (in mM: 205 sucrose, 10 glucose, 26 $NaHCO_3$, 1.2 $NaH_2PO_4.H_2O$, 2.5 KCl, 5 $MgCl_2$, and 0.1 $CaCl_2$) and horizontal slices cut at 300 µm thickness. Recordings used a membrane chamber (78, 79) perfused with oxygenated ACSF at 16 mL/min and heated to 34 °C. Patch-clamp recordings used a ~5 MΩ glass microelectrode filled with intracellular solution (in mM: 135 K-gluconate, 4 KCl, 10 4-(2-Hydroxyethyl)piperazine-1-ethanesulfonic acid (HEPES), 4 Mg-ATP, 0.3 Na-GTP, 10 Na_2-phosphocreatine; pH 7.3; 290 mOsm). Approximately 5 minutes after achieving whole-cell configuration, a series of current steps (100 ms with 1 s between steps, −100 to +400 pA in 25 pA increments) were applied. The first action potential evoked by a depolarizing current was selected for analysis. Recordings were rejected if access resistance was >20 MΩ. Signal was acquired using a MultiClamp 700B amplifier (Molecular Devices), Power 1401 digitizer [Cambridge Electronic Design (CED)] and Signal software (v6, CED). Signals were digitized at 25 kHz and low-pass filtered at 10 kHz. Action potential data were analyzed using custom-MATLAB scripts (10).

Recording of Sodium Currents (I_{Na}) in Human iPSC-Derived Neurons. Studies involving iPSCs were reviewed and approved by the RCSI Research Ethics Committee under approval REC202302020. Human iPSCs, derived from a healthy female adult, were obtained from a biobank (cell line HPSI0114i-eipl_1 ECACC 77650081; Culture Collections, Public Health England; https://hpscreg.eu/cell-line/WTSIi020-A). Informed consent was obtained for the donation of the skin sample from which the cell line was generated. Cells were differentiated for 1 mo into glutamatergic and GABAergic neurons in vitro and then treated with Ant-335 or scramble for 48 h. Cells used for qRT-PCR were processed as above. For patch recordings, cells were dissociated with Accutase (BioLegend) and plated on plastic coverslips. I_{Na} were recorded using MultiClamp 700B amplifier, pCLAMP 11 software, and a Digidata 1550B (from Molecular Devices). Currents were low-pass filtered at 10 kHz and sampled at 50 kHz. Borosilicate electrodes (3 to 5 MΩ) were filled with (in mM): 100 CsF, 25 TEA-Cl, 10 NaCl, 10 HEPES, 1 EGTA, 1 $MgCl_2$, 4 Mg-ATP, and 0.4 Na-GTP (pH to 7.3 with CsOH, 290 mOsm/kg). Neurons were superfused with (in mM): 110 NaCl, 30 TEA-Cl, 10 4-aminopyridine (4-AP), 10 HEPES, 10 glucose, 1.6 $CaCl_2$, 1 $MgCl_2$, and 0.2 $CdCl_2$ (pH to 7.4 with NaOH, 300 mOsm/kg). All experiments were performed at 34 °C. A minimum series resistance compensation of 70% was applied. Capacitive and leak currents were subtracted using the P/N-4 protocol. The current–voltage relationship was determined using a series of 100-ms voltage pulses from a holding potential of −110 mV to 0 mV in steps of 10 mV increments at 10 s intervals. I_{Na} current density was calculated by dividing the maximal current amplitude by the cell capacitance.

iCLIP. Ethical approval for the donation of brain tissue samples was provided by the Ethics Commission of the Faculty of Medicine, Goethe University Frankfurt, Frankfurt am Main, Germany (#4/09). Consent was obtained according to the Declaration of Helsinki from all participants. Tissues were ruptured and cross-linked by ultraviolet light at 254 nm. Cells were subjected to AGO2 immunoprecipitation (*SI Appendix*), followed by SDS-page and proteinase K digestion to elute out cross-linked protein/RNA complex. The complex was circularized to form the AGO2 iCLIP library for high-throughput sequencing (Illumina NextSeq 500 sequencer). The iCLIP data were adapter trimmed, demultiplexed and quality filtered, identical reads collapsed to remove PCR bias and unique molecular identifier (UMI) sequences were removed. Reads were mapped to the human genome using Bowtie2 with soft-clipping enabled. Only uniquely mapping reads were used for further steps. Cross-linking sites in the human genome (GRCh38) were found, with the assumption that sequencing reads start exactly one position downstream of the cross-linked nucleotide. According to the genomic sequence, 10 bp was added to each side of cross-linking sites and CLIPper (https://github.com/YeoLab/clipper) (80) was used to detect significant iCLIP peaks. miRNAs sequenced in the iCLIP data were quantified by mapping with Bowtie2 (soft-clipping enabled) to mature human miRNAs from miRBase v22 (69). MiRNA target interactions (MTIs) were employed to search for seed-complementary sites. Only one MTI was permitted per iCLIP peak. Identified MTIs were intersected with predicted miRNA targets from TargetScanHuman version 7.0 to obtain the overlap of predicted and detected MTIs (81). Only genes with 7mer-A1, 7mer-m8, and 8mer binding sites were considered as the validated targets.

Statistical Analysis. All statistical analyses were performed using GraphPad Prism (version 9). Data were tested for normal distribution using the D'Agostino and Pearson omnibus normality test or Shapiro-Wilk test for small n numbers. Parametric statistics used an unpaired two-tailed Student's *t* test (with Welch correction when assuming nonequal SEM) and data are presented as mean ± SEM. Nonparametric analyses used the Mann–Whitney *U* test, and data are presented as median ± interquartile range. For comparison of data with multiple parameters, a two-way repeated measures ANOVA was used. The individual tests used for each comparison are specified in the text. Data were considered significant at P value ≤ 0.05. Corrections were performed on data with multiple comparisons. The adjusted alpha is specified in the text.

Data, Materials, and Software Availability. The sequencing and iCLIP data reported in this paper have been deposited to the gene expression omnibus (GEO) under accession number GSE214355 (82) (Argonaute2 sequencing of hippocampal subfields from rat PPS epilepsy model), GSE214761 (83) (CBD small RNA sequencing), and GSE214317 (84) (Ago iCLIP of the TLE patient resected hippocampus). Custom analysis codes are available in GitHub at https://github.com/niamhconno/Heiland-et-al-2022 (85). All other data are included in the manuscript and/or supporting information.

ACKNOWLEDGMENTS. This publication has emanated from research supported by a research grant from Science Foundation Ireland (SFI) under grant 16/RC/3948 (FutureNeuro), the European Union's "Seventh Framework" Programme (FP7) under Grant Agreement 602130 (EpimiRNA), the Wellcome Trust (222648/Z/21/Z) and the Higher Education Authority (HEA), Department of Further and Higher Education, Research, Innovation & Science (DFHERIS) and the Shared Island Fund (SeeDeepER). G.M. was supported by fellowships from the European Union (MSCA-IF-2018 840262) and Epilepsy Research UK (F2102 Morris) and by the Royal Society (RGS\R2\222326), and J.C.K. by SFI award 17/CDA/4708. We thank STI pharmaceuticals Ltd. (UK) and PureForm Global Inc (USA) for providing the cannabidiol.

Author affiliations: [a]Department of Physiology and Medical Physics, Royal College of Surgeons in Ireland, University of Medicine and Health Sciences, Dublin D02 YN77, Ireland; [b]FutureNeuro Science Foundation Ireland Research Centre, Royal College of Surgeons in Ireland, University of Medicine and Health Sciences, Dublin D02 YN77, Ireland; [c]Interdisciplinary Nanoscience Centre, Aarhus University, 8000 Aarhus C, Denmark; [d]Department of Molecular Biology and Genetics, Aarhus University, 8000 Aarhus C, Denmark; [e]Omiics, 8200 Aarhus N, Denmark; [f]Epilepsy Center, Department of Neurology, Philipps University Marburg, Marburg 35043, Germany; [g]Epilepsy Center Frankfurt Rhine-Main, Department of Neurology, University Hospital Frankfurt, Frankfurt a.M. 60528, Germany; [h]Landes-Offensive zur Entwicklung Wissenschaftlich-ökonomischer Exzellenz, Center for Personalized Translational Epilepsy Research, Goethe-University Frankfurt, Frankfurt a.M. 60528, Germany; [i]Department of Neurosurgery, University of Rostock, Rostock 18057, Germany; [j]Institute of Molecular Medicine, University of Southern Denmark, 5000 Odense, Denmark; [k]Wellcome-Wolfson Institute for Experimental Medicine, School of Medicine, Dentistry and Biomedical Science, Queens University, Belfast BT9 7BL, United Kingdom; [l]Danish Institute for Advanced Study, University of Southern Denmark, 5230 Odense, Denmark; [m]Department of Clinical Genetics, Odense University Hospital, 5000 Odense, Denmark; and [n]Department of Neuroscience, Physiology and Pharmacology, University College London, London WC1E 6BT, United Kingdom

Author contributions: M.H., T.E., T.D.M.H., V.K.T., F.R., S.B., J.K., G.M., and D.C.H. designed research; M.H., N.M.C.C., O.M., J.C.K., E.L., Y.Y., J.S., M.T.V., L.S.C., V.N., T.M.F., A.M., V.K.T., and G.M. performed research; M.H., N.M.C.C., N.T.N., J.C.K., K.F., A.S., Y.Y., M.T.V., L.S.C., V.N., and G.M. analyzed data; and M.H., G.M., and D.C.H. wrote the paper.

Competing interest statement: RCSI University of Medicine and Health Sciences (D.C.H., G.M., and M.H.) reports the European Patent Application No. EP21198390.3 "Modulation of microRNA-335-5p for the treatment of sodium channelopathies."

1. R. S. Fisher *et al.*, ILAE official report: A practical clinical definition of epilepsy. *Epilepsia* **55**, 475–482 (2014).
2. W. Löscher, P. Klein, The Pharmacology and Clinical Efficacy of Antiseizure Medications: From Bromide Salts to Cenobamate and Beyond. *CNS Drugs* **35**, 935–963 (2021).
3. M. J. Brodie, Sodium Channel Blockers in the Treatment of Epilepsy. *CNS Drugs* **31**, 527–534 (2017).
4. M. H. Meisler, S. F. Hill, W. Yu, Sodium channelopathies in neurodevelopmental disorders. *Nat. Rev. Neurosci.* **22**, 152–166 (2021).
5. D. Steel, J. D. Symonds, S. M. Zuberi, A. Brunklaus, Dravet syndrome and its mimics: Beyond SCN1A. *Epilepsia* **58**, 1807–1816 (2017).
6. A. Eulalio, E. Huntzinger, E. Izaurralde, Getting to the root of miRNA-mediated gene silencing. *Cell* **132**, 9–14 (2008).
7. D. P. Bartel, MicroRNAs: Genomics, biogenesis, mechanism, and function. *Cell* **116**, 261–297 (2004).
8. W. A. Alsharafi, B. Xiao, M. M. Abuhamed, Z. Luo, miRNAs: Biological and clinical determinants in epilepsy. *Front. Mol. Neurosci.* **8**, 59 (2015).
9. G. P. Brennan, D. C. Henshall, MicroRNAs as regulators of brain function and targets for treatment of epilepsy. *Nat. Rev. Neurol.* **16**, 506–519 (2020).
10. M. T. Veno *et al.*, A systems approach delivers a functional microRNA catalog and expanded targets for seizure suppression in temporal lobe epilepsy. *Proc. Natl. Acad. Sci. U.S.A.* **117**, 15977–15988 (2020).
11. E. M. Jimenez-Mateos *et al.*, Silencing microRNA-134 produces neuroprotective and prolonged seizure-suppressive effects. *Nat. Med.* **18**, 1087–1094 (2012).
12. M. E. Peter, Targeting of mRNAs by multiple miRNAs: The next step. *Oncogene* **29**, 2161–2164 (2010).
13. G. Servilha-Menezes, N. Garcia-Cairasco, A complex systems view on the current hypotheses of epilepsy pharmacoresistance. *Epilepsia Open* **7** (Suppl 1), S8–S22 (2022).
14. C. Gross, D. Tiwari, Regulation of ion channels by microRNAs and the implication for epilepsy. *Curr. Neurol. Neurosci. Rep.* **18**, 60 (2018).
15. G. Morris, MicroRNAs - small RNAs with a big influence on brain excitability. *J. Physiol.* **601**, 1711–1718 (2023), 10.1113/JP283719.
16. N. M. Sosanya *et al.*, Degradation of high affinity HuD targets releases Kv1.1 mRNA from miR-129 repression by mTORC1. *J. Cell Biol.* **202**, 53–69 (2013).
17. C. Gross *et al.*, MicroRNA-mediated downregulation of the potassium channel Kv4.2 contributes to seizure onset. *Cell Rep.* **17**, 37–45 (2016).
18. D. Tiwari *et al.*, MicroRNA inhibition upregulates hippocampal A-type potassium current and reduces seizure frequency in a mouse model of epilepsy. *Neurobiol. Dis.* **130**, 104508 (2019).
19. Z. Zhang, Z. Wang, B. Zhang, Y. Liu, Downregulation of microRNA155 by preoperative administration of valproic acid prevents postoperative seizures by upregulating SCN1A. *Mol. Med. Rep.* **17**, 1375–1381 (2018).
20. A. Campbell *et al.*, AntimiR targeting of microRNA-134 reduces seizures in a mouse model of Angelman syndrome. *Mol. Ther Nucleic Acids* **28**, 514–529 (2022).
21. U. Bekenstein *et al.*, Dynamic changes in murine forebrain miR-211 expression associate with cholinergic imbalances and epileptiform activity. *Proc. Natl. Acad. Sci. U.S.A.* **114**, E4996–E5005 (2017).
22. GWPharmaceuticals, EPIDOLEX (cannabidiol) Oral Solution - the first FDA-approved plant-derived cannabinoid medicine - now available by prescription in the U.S. (2018).
23. GWPharmaceuticals, GW Pharmaceuticals receives European Commission approval for EPIDOLEX (cannabidiol) for the treatment of seizures in patients with two rare, severe forms of childhood-onset epilepsy. (2019).
24. E. Aronica *et al.*, Expression pattern of miR-146a, an inflammation-associated microRNA, in experimental and human temporal lobe epilepsy. *Eur. J. Neurosci.* **31**, 1100–1107 (2010).
25. F. He *et al.*, Modulation of miR-146a/complement factor H-mediated inflammatory responses in a rat model of temporal lobe epilepsy. *Biosci. Rep.* **36**, e00433 (2016).
26. R. Raoof *et al.*, Dual-center, dual-platform microRNA profiling identifies potential plasma biomarkers of adult temporal lobe epilepsy. *EBioMedicine* **38**, 127–141 (2018).
27. R. C. McKiernan *et al.*, Reduced mature microRNA levels in association with dicer loss in human temporal lobe epilepsy with hippocampal sclerosis. *PLoS One* **7**, e35921 (2012).
28. N. Ludwig *et al.*, Distribution of miRNA expression across human tissues. *Nucleic Acids Res.* **44**, 3865–3877 (2016).
29. A. Keller *et al.*, miRNATissueAtlas2: An update to the human miRNA tissue atlas. *Nucleic Acids Res.* **50**, D211–D221 (2022).
30. C. H. Chou *et al.*, miRTarBase update 2018: A resource for experimentally validated microRNA-target interactions. *Nucleic Acids Res.* **46**, D296–D302 (2018).
31. D. Karagkouni *et al.*, DIANA-TarBase v8: A decade-long collection of experimentally supported miRNA-gene interactions. *Nucleic Acids Res.* **46**, D239–D245 (2018).
32. T. Tokar *et al.*, mirDIP 4.1-integrative database of human microRNA target predictions. *Nucleic Acids Res.* **46**, D360–D370 (2018).
33. J. Konig *et al.*, iCLIP reveals the function of hnRNP particles in splicing at individual nucleotide resolution. *Nat. Struct. Mol. Biol.* **17**, 909–915 (2010).
34. M. M. Salman *et al.*, Transcriptome analysis suggests a role for the differential expression of cerebral aquaporins and the MAPK signalling pathway in human temporal lobe epilepsy. *Eur. J. Neurosci.* **46**, 2121–2132 (2017).
35. M. Mantegazza, S. Cestele, W. A. Catterall, Sodium channelopathies of skeletal muscle and brain. *Physiol. Rev.* **101**, 1633–1689 (2021).
36. L. Kandratavicius *et al.*, Animal models of epilepsy: Use and limitations. *Neuropsychiatr. Dis. Treat* **10**, 1693–1705 (2014).
37. G. Morris, D. O'Brien, D. C. Henshall, Opportunities and challenges for microRNA-targeting therapeutics for epilepsy. *Trends Pharmacol. Sci.* **42**, 605–616 (2021).
38. N. A. Jones *et al.*, Cannabidiol displays antiepileptiform and antiseizure properties in vitro and in vivo. *J. Pharmacol. Exp. Ther.* **332**, 569–577 (2010).
39. K. W. Kim *et al.*, Posttranscriptional modulation of KCNQ2 gene expression by the miR-106b microRNA family. *Proc. Natl. Acad. Sci. U.S.A.* **118**, e2110200118 (2021).
40. A. Korotkov, J. D. Mills, J. A. Gorter, E. A. van Vliet, E. Aronica, Systematic review and meta-analysis of differentially expressed miRNAs in experimental and human temporal lobe epilepsy. *Sci. Rep.* **7**, 11592 (2017).
41. P. K. Srivastava *et al.*, Meta-analysis of microRNAs dysregulated in the hippocampal dentate gyrus of animal models of epilepsy. *eNeuro* **4** (2017).
42. P. Bencurova *et al.*, Dynamic miRNA changes during the process of epileptogenesis in an infantile and adult-onset model. *Sci. Rep.* **11**, 9649 (2021).
43. M. Schouten *et al.*, MicroRNA-124 and -137 cooperativity controls caspase-3 activity through BCL2L13 in hippocampal neural stem cells. *Sci. Rep.* **5**, 12448 (2015).
44. A. M. Bot, K. J. Debski, K. Lukasiuk, Alterations in miRNA levels in the dentate gyrus in epileptic rats. *PLoS One* **8**, e76051 (2013).
45. J. A. Gorter *et al.*, Hippocampal subregion-specific microRNA expression during epileptogenesis in experimental temporal lobe epilepsy. *Neurobiol. Dis.* **62**, 508–520 (2014).
46. L. G. L. Antonio *et al.*, Expression of microRNAs miR-145, miR-181c, miR-199a and miR-1183 in the blood and hippocampus of patients with mesial temporal lobe epilepsy. *J. Mol. Neurosci.* **69**, 580–587 (2019).
47. R. Surges *et al.*, Changes in serum miRNAs following generalized convulsive seizures in human mesial temporal lobe epilepsy. *Biochem. Biophys. Res. Commun.* **481**, 13–18 (2016).
48. D. Gattás *et al.*, MicroRNAs miR-629-3p, miR-1202 and miR-1225-5p as potential diagnostic and surgery outcome biomarkers for mesial temporal lobe epilepsy with hippocampal sclerosis. *Neurochirurgie* **68**, 583–588 (2022).
49. L. F. Almeida Silva *et al.*, Genetic deletion of microRNA-22 blunts the inflammatory transcriptional response to status epilepticus and exacerbates epilepsy in mice. *Mol. Brain* **13**, 114 (2020).
50. C. L. Tan *et al.*, MicroRNA-128 governs neuronal excitability and motor behavior in mice. *Science* **342**, 1254–1258 (2013).
51. A. L. Hodgkin, A. F. Huxley, A quantitative description of membrane current and its application to conduction and excitation in nerve. *J. Physiol.* **117**, 500–544 (1952).
52. J. Du *et al.*, Differential excitatory vs inhibitory SCN expression at single cell level regulates brain sodium channel function in neurodevelopmental disorders. *Eur. J. Paediatr Neurol.* **24**, 129–133 (2020).
53. F. H. Yu *et al.*, Reduced sodium current in GABAergic interneurons in a mouse model of severe myoclonic epilepsy in infancy. *Nat. Neurosci.* **9**, 1142–1149 (2006).
54. M. Mantegazza, G. Curia, G. Biagini, D. S. Ragsdale, M. Avoli, Voltage-gated sodium channels as therapeutic targets in epilepsy and other neurological disorders. *Lancet Neurol.* **9**, 413–424 (2010).
55. S. Kumar, M. Megha, B. Chogtu, K. L. Bairy, Effect of acute and chronic administration of losartan, atorvastatin and their combination on animal models of epilepsy. *Res. J. Pharmaceutical, Biol. Chem. Sci.* **6**, 1795–1801 (2015).
56. K. V. Reddy, M. A. Kumar, G. V. Kumar, Isradipine enhances the anticonvulsant activity of carbamazepine against MES and PTZ induced convulsions in rats. *IJPSR* **6**, 247–250 (2015).
57. T. C. Roberts, R. Langer, M. J. A. Wood, Advances in oligonucleotide drug delivery. *Nat. Rev. Drug Discov.* **19**, 673–694 (2020).
58. J. Ziobro, K. Eschbach, J. E. Sullivan, K. G. Knupp, Current treatment strategies and future treatment options for Dravet syndrome. *Curr. Treat Options Neurol.* **20**, 52 (2018).
59. A. Strzelczyk, S. Schubert-Bast, Therapeutic advances in Dravet syndrome: A targeted literature review. *Expert Rev. Neurother.* **20**, 1065–1079 (2020).
60. A. S. Nudelman *et al.*, Neuronal activity rapidly induces transcription of the CREB-regulated microRNA-132, in vivo. *Hippocampus* **20**, 492–498 (2010).
61. E. M. Jimenez-Mateos *et al.*, miRNA Expression profile after status epilepticus and hippocampal neuroprotection by targeting miR-132. *Am. J. Pathol.* **179**, 2519–2532 (2011).
62. F. Capitano *et al.*, MicroRNA-335-5p modulates spatial memory and hippocampal synaptic plasticity. *Neurobiol. Learn Mem.* **139**, 63–68 (2017).
63. W. Si *et al.*, miR-335 promotes stress granule formation to inhibit apoptosis by targeting ROCK2 in acute ischemic stroke. *Int. J. Mol. Med.* **43**, 1452–1466 (2019).
64. J. Li, H. Meng, W. Cao, T. Qiu, MiR-335 is involved in major depression disorder and antidepressant treatment through targeting GRM4. *Neurosci. Lett.* **606**, 167–172 (2015).
65. R. J. Racine, Modification of seizure activity by electrical stimulation. II. Motor seizure. *Electroencephal. Clin. Neurophysiol.* **32**, 281–294 (1972).
66. M. Pohl, P. Mares, Effects of flunarizine on Metrazol-induced seizures in developing rats. *Epilepsy Res.* **1**, 302–305 (1987).
67. L. Stoica, S. S. Ahmed, G. Gao, M. Sena-Esteves, Gene transfer to the CNS using recombinant adeno-associated virus. *Curr. Protoc. Microbiol.* Chapter 14, Unit14D 15 (2013).
68. Z. Gu, R. Eils, M. Schlesner, Complex heatmaps reveal patterns and correlations in multidimensional genomic data. *Bioinformatics* **32**, 2847–2849 (2016).
69. A. Kozomara, M. Birgaoanu, S. Griffiths-Jones, miRBase: From microRNA sequences to function. *Nucleic Acids Res.* **47**, D155–D162 (2019).
70. P. J. Thul *et al.*, A subcellular map of the human proteome. *Science* **356**, eaal3321 (2017).
71. N. C. Tan, S. F. Berkovic, The Epilepsy Genetic Association Database (epiGAD): Analysis of 165 genetic association studies, 1996–2008. *Epilepsia* **51**, 686–689 (2010).
72. J. Wang *et al.*, Epilepsy-associated genes. *Seizure* **44**, 11–20 (2017).
73. A. P. Davis *et al.*, The comparative toxicogenomics database: Update 2019. *Nucleic Acids Res.* **47**, D948–D954 (2019).
74. G. Yu, Q. Y. He, ReactomePA: An R/Bioconductor package for reactome pathway analysis and visualization. *Mol. Biosyst.* **12**, 477–479 (2016).
75. G. Yu, L. G. Wang, Y. Han, Q. Y. He, clusterProfiler: An R package for comparing biological themes among gene clusters. *OMICS* **16**, 284–287 (2012).
76. R. C. Team, R: A language and environment for statistical computing. R Foundation for Statistical Computing, Vienna. (version 4.1.3, 2022), https://www.R-project.org.
77. H. Wickham, The split-apply-combine strategy for data analysis. *J. Stat. Software* **40**, 1–29 (2011).
78. G. Morris, P. Jiruska, J. G. Jefferys, A. D. Powell, A new approach of modified submerged patch clamp recording reveals interneuronal dynamics during epileptiform oscillations. *Front Neurosci.* **10**, 519 (2016).
79. M. R. Hill, S. A. Greenfield, The membrane chamber: A new type of in vitro recording chamber. *J. Neurosci. Methods* **195**, 15–23 (2011).
80. M. T. Lovci *et al.*, Rbfox proteins regulate alternative mRNA splicing through evolutionarily conserved RNA bridges. *Nat. Struct. Mol. Biol.* **20**, 1434–1442 (2013).
81. V. Agarwal, G. W. Bell, J. W. Nam, D. P. Bartel, Predicting effective microRNA target sites in mammalian mRNAs. *Elife* **4**, e05005 (2015).
82. M. T. Veno, J. Kjems, D. C. Henshall, Argonaute 2 associated miRNAs in CA1, CA3 and Dentate Gyrus hippocampal subfields from the rat perforant pathway stimulation (PPS) epilepsy model. NCBI Gene Expression Omnibus. https://www.ncbi.nlm.nih.gov/geo/query/acc.cgi?acc=GSE214355. Deposited 28 September 2022.
83. M. Heiland, N. T. Nguyen, D. C. Henshall, Effects of cannabidiol on miRNA expression in naïve mice. NCBI Gene Expression Omnibus. https://www.ncbi.nlm.nih.gov/geo/query/acc.cgi?acc=GSE214761. Deposited 4 October 2022.
84. M. T. Veno, J. Kjems, S. Bauer, F. Rosenow, Ago iCLIP of TLE patient resected hippocampus. NCBI Gene Expression Omnibus. https://www.ncbi.nlm.nih.gov/geo/query/acc.cgi?acc=GSE214317. Deposited 27 September 2022.
85. N. M. C. Connolly, R code and accompanying files to reproduce miRNA target investigation and pathway enrichment analysis. Github. https://github.com/niamhconno/Heiland-et-al-2022. Deposited 29 September 2022.